PERGAMON

Journal of Structural Geology 22 (2000) 913–930

JOURNAL OF STRUCTURAL GEOLOGY

www.elsevier.nl/locate/jstrugeo

Mesoscopic structure of the Punchbowl Fault, Southern California and the geologic and geophysical structure of active strike-slip faults

Steven E. Schulz [1], James P. Evans*

Department of Geology, Utah State University, Logan, UT 84322-4505, USA

Received 15 June 1999; accepted 2 March 2000

Abstract

We examine the distribution, density, and orientation of outcrop-scale structures related to the Punchbowl Fault, an exhumed ancient trace of the San Andreas Fault, southern California, in order to determine the structure of the fault zone. The Punchbowl Fault has 44 km of right-lateral slip, and cuts the Cretaceous Pelona Schist in the study area. The mesoscopic structures examined include fractures, small faults, and veins; they were inventoried using scan lines at closely spaced stations along three strike-perpendicular traverses 200–250 m long across the fault. The fault zone thickness is a function of the type of structure measured. Slip along narrow (<2 m wide) ultracataclasite cores of the faults results in foliation reorientation over a distance of 50 m from the cores: fracture and fault densities appear to increase 50–80 m from the fault cores, and vein densities are highly variable across the fault zone. Fractures and faults in the damaged zone have a variety of orientations, but most are at high angles to the main fault zone. When coupled with previous geochemical and microstructural data, these data show that large-displacement faults of the San Andreas system, are up to 200–250 m thick, and enclose zones of mineralogic and geochemical alteration that are 20–30 m thick. Extreme slip localization occurs over zones 1–5 m thick. When reconciled with geophysical imaging, our data suggest that trapped headwaves travel in the damaged zone, and that some aftershock events produce slip on faults and fractures, which often have orientations very different from the principal slip surfaces.

1. Introduction

Evaluating the mesoscopic structure of fault zones at scales of between one meter and hundreds of meters is important for a variety of applications, including hydrogeology (Forster and Evans, 1991; Haneberg, 1995; Lopez and Smith, 1995; Caine et al., 1996; Zhang and Sanderson, 1996; Matthai et al., 1998), hydrocarbon migration (Fisher and Knipe, 1998), waste isolation (Ferrill et al., 1999), ore deposits (Guilbert and Park, 1985; Sibson et al., 1988), earthquake nucleation and propagation (Sibson, 1989; Li et al., 1998), and the rheological/mechanical behavior of faults (Bruhn et al., 1994). Chester and Logan (1986) suggested that the three important mechanical, hydrologic, and structural entities in and around a fault zone are the protolith, the damaged zone, and fault core. The damaged zone consists of the region of deformation associated with the fault, and may consist of an increased concentration of fractures, faults, veins, and microstructural deformation (Chester et al., 1993; Goddard and Evans, 1995; Caine and Forster, 1999). The fault core is the portion of the fault which consists of highly deformed rock where much of the slip is accommodated (Chester et al., 1993). Where such tripartaite division of fault rock types exist, they are likely to have significant impacts on the mechanical and hydrologic behavior of faults (Bruhn et al., 1994;

* Corresponding author. Tel: +1-435-797-1267; fax: +1-435-797-1588.

E-mail address: jpevans@cc.usu.edu (J.P. Evans).

[1] Now at: Marathon Oil Co., Houston, TX, USA.

0191-8141/00/$ - see front matter
PII: S0191-8141(00)00019-5

Evans et al., 1997), as well as produce important, recognizable geophysical and geochemical signatures. (e.g. Li et al., 1994a,b; Unsworth et al., 1999).

To date, most work on exhumed fault structure has focused on individual aspects of faulting, and little work has related data on the structure, mechanics, mechanisms and morphology of fault zones across a range of depths and scales, or considered how fault structure influences earthquake wave propagation and fault segmentation. The San Andreas Fault (SAF) is perhaps the most intensively studied fault zone in the world, with a variety of geological and geophysical investigations of the processes of seismic slip, rupture, and segmentation. Geologic studies of exhumed faults in the SAF system (Waters and Campbell, 1935; Oakshott, 1958; Anderson et al., 1980, 1983; Chester et al., 1993; Evans and Chester, 1995) suggest that to at least 4 km depth, major faults of the SAF system are limited to thin, discrete slip surfaces commonly within a fractured zone up to 200 m wide. There may be multiple anastomosing slip surfaces that are confined to a relatively thin zone, outside of which there is little to no fault-related deformation (Chester et al., 1993). These slip zones are interpreted as being bounded by zones of enhanced deformation, as suggested by increased densities of fractures, veins, and small faults.

We examine the variation of mesoscopic structures across the Punchbowl Fault, an exhumed ancient trace of the SAF, developed in metamorphic rocks, and combine these data with previous investigations to evaluate how a fault zone may be imaged by direct and indirect methods. We examined the Punchbowl Fault at multiple scales from mesoscopic (outcrop) to microscopic (petrographic and scanning electron microscopes). The density and orientations of fractures, veins, and small faults and the reorientation of pre-fault schistosity were documented along traverses perpendicular to the fault zone and are presented in this paper. The geochemical, microstructural and mineralogical variations within the fault zone are summarized in Schulz and Evans (1998). In this paper we briefly describe our methods for detailed outcrop analyses of fault zones, then present our results, which consist of the qualitative description of the rocks, followed by the analysis of the quantitative data. Finally, we discuss the structural and geophysical implications of our results.

2. Geologic setting

Much of the geologic setting of the study area has been described by Schulz and Evans (1998), and is briefly summarized here. The SAF is a right-lateral strike-slip fault that is part of a system of faults that forms the boundary between the Pacific and North American plates (Wallace, 1990; Powell and Weldon, 1992; Powell, 1993). Two of the larger and better exposed inactive traces of the SAF are the San Gabriel and Punchbowl Faults, which lie south of the Mojave segment of the SAF in the San Gabriel Mountains (Fig. 1, inset). The Punchbowl Fault was active from 4 Ma to 1 Ma and has a total right-lateral displacement of 44 km (Dibblee, 1968; Ehlig, 1981; Weldon et al., 1993). Right-lateral slip on the Punchbowl Fault was abandoned in favor of slip along the SAF (Powell and Weldon, 1992). Uplift of the San Gabriel Mountains (Ehlig, 1981; Anderson et al., 1983) resulted in exhumation of the Punchbowl Fault by at least 2–4 km (Noble, 1954; Chester and Logan, 1986). The top of the seismicity along the modern SAF is ~2–4 km. Thus, the Punchbowl Fault zone is likely to be an exhumed analog of the SAF. The type and spatial distribution of macroscopic and microscopic structures associated with the Punchbowl Fault offer an indication of the fault-zone characteristics found at seismogenic depths along the SAF.

The study area lies astride the Punchbowl Fault near Wrightwood, California (Fig. 1) and extends from Devil's Punchbowl County Park (site of the Chester and Logan, 1986, 1987 studies) in the west to Cajon Pass in the east. Northwest of the study region, the fault strikes 294° and dips 70°SW on average, with a variation of 15° in strike and 26° in dip over a distance of roughly 6 km. The slip direction rakes 30° SE (Chester and Logan, 1987) and the fault juxtaposes the Tertiary Punchbowl Formation against older crystalline basement rock (Noble, 1954; Dibblee, 1968; Chester and Logan, 1986).

In much of the present study area, the Punchbowl Fault has at least two main traces (Fig. 1; Jacobson, 1983a; Dibblee, 1987; Ehlig, 1987; Weldon et al., 1993). The rocks between the two traces in the study area are limited to the Punchbowl Formation, Pelona Schist, and an aplite unit. In the middle portion of the field area the Punchbowl Fault has been mapped as only a single strand (Noble, 1954; Ehlig, 1981). However, the fault in this area is not well exposed, and more than one major strand may be present. At the eastern end of the study area, Powell and Weldon (1992) identified multiple strands of the fault (Fig. 1) that merge with the active trace of the SAF and the San Jacinto Fault. No evidence exists to determine the relative timing of motion on the two strands.

The Pelona Schist consists of two rock types. It is dominated by a metagreywacke, which is an albite–quartz–muscovite schist with minor epidote, graphite, and chlorite. Smaller amounts of greenschist interpreted to be a metavolcanic sequence of albite–chlorite–clinozoisite–actinolite are found in the region. Relatively rare occurrences of calcite–marble, quartzite, and local masses of coarse actinolite and talc

schist also are found (Ehlig, 1958; Dibblee, 1967; Jacobson, 1980; Haxel et al., 1987; Jacobson et al., 1988; Jacobson, 1990). In our study area, rocks north of the Punchbowl Fault are dominated by the greenschists, and by greyschists south of the fault zone. Aplite to granophyric quartz monzonite dikes are also common in the study area. The age of metamorphism is thought to be Late Cretaceous (Jacobson, 1990).

Three traverses were examined in detail for this study (Fig. 1). The three sites chosen all have at least one fault core exposed and have reasonably good exposure of the fault zone and the host rock. Traverses 1 and 2 are in areas where the Punchbowl Fault has been mapped by Ehlig (1987) as two main branches.

The north branch of the Punchbowl Fault is exposed at traverse 1, along with the wall-rocks from between the two main fault branches (Figs. 1 and 2a). Both branches of the Punchbowl Fault are well exposed at traverse 2 (Fig. 2b). The fault core of the north branch is not exposed, but its location can be determined to within 5 m by a change in lithology. The protolith north of the northern branch of the fault core is well exposed for over 100 m. The rocks to the south of the southern branch of the fault core are poorly exposed, but the limited outcrop enables some analysis of the rocks.

Traverse 3 is 12 km southeast of traverse 2 (Fig. 1), where a large road cut exposes the Punchbowl Fault at the south end and the SAF at the north end. Over 100 m of continuous, undeformed Pelona Schist south of the Punchbowl Fault is exposed, and there is a sharp contact in the intensely deformed rocks of the fault. Work on the 130-m-long traverse 3 was limited to the southern branch of the Punchbowl Fault and the undeformed rocks to the south (Fig. 2c). Traverse 1 is oriented approximately north–south, and is ~80° from the trace of the fault. Traverse 2 is oriented N 30° E and also makes an angle of ~30° with the fault. Tra-

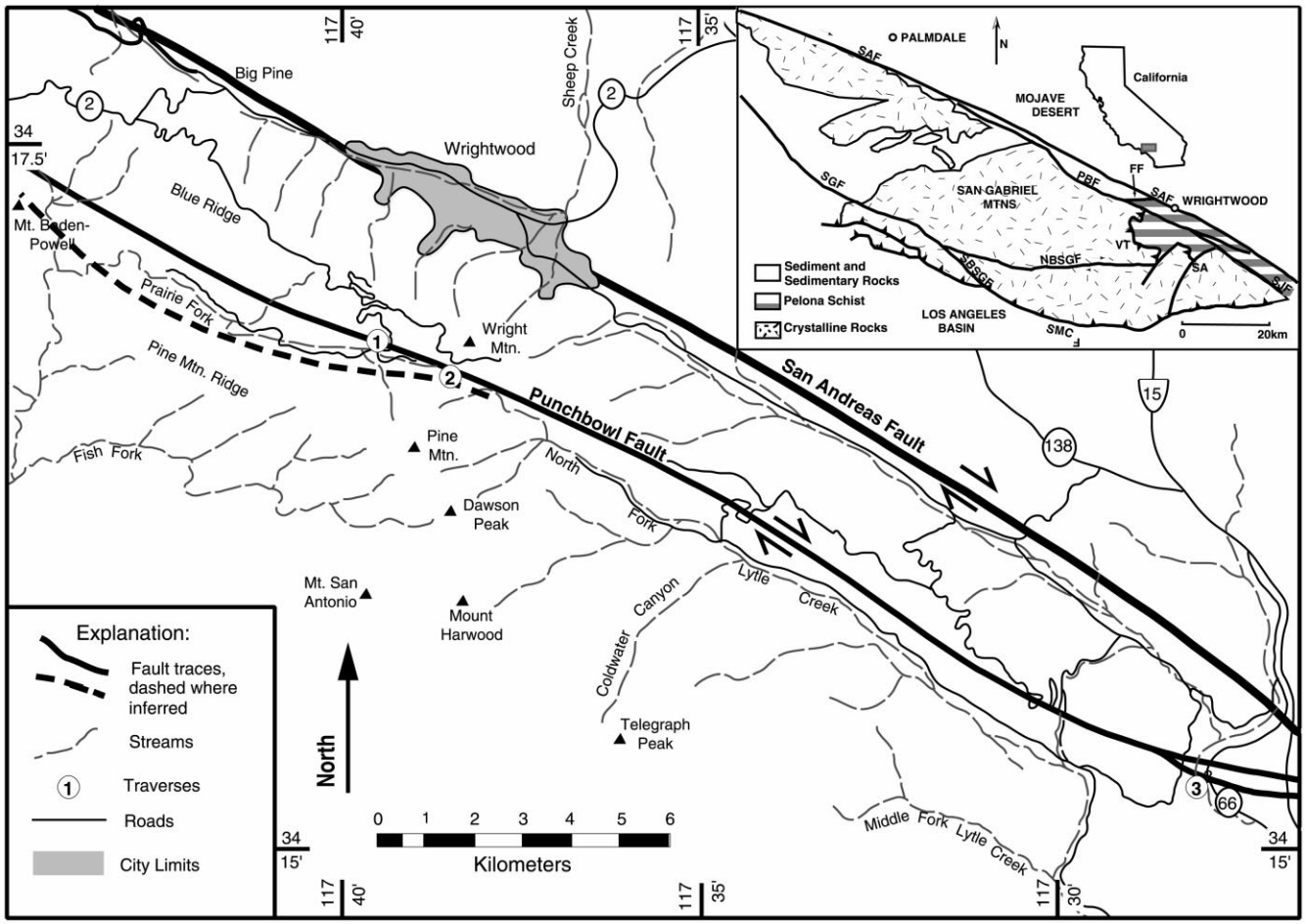

Fig. 1. Location map of the study region in the San Gabriel Mountains, southern California. Inset shows the location of the San Gabriel range and the major tectonic elements of the area. The locations of the three traverses along the Punchbowl Fault are indicated. Major faults are labeled; SAF—San Andreas Fault, PBF—Punchbowl Fault, SGF—San Gabriel Fault, NBSGF—north branch of the San Gabriel Fault, SBSGF—south branch of the San Gabriel Fault, SMCF—Sierra Madre–Cucamonga Fault, SA—San Antonio Fault, FF—Fenner Fault, SJF—San Jacinto Fault, VT—Vincent Thrust.

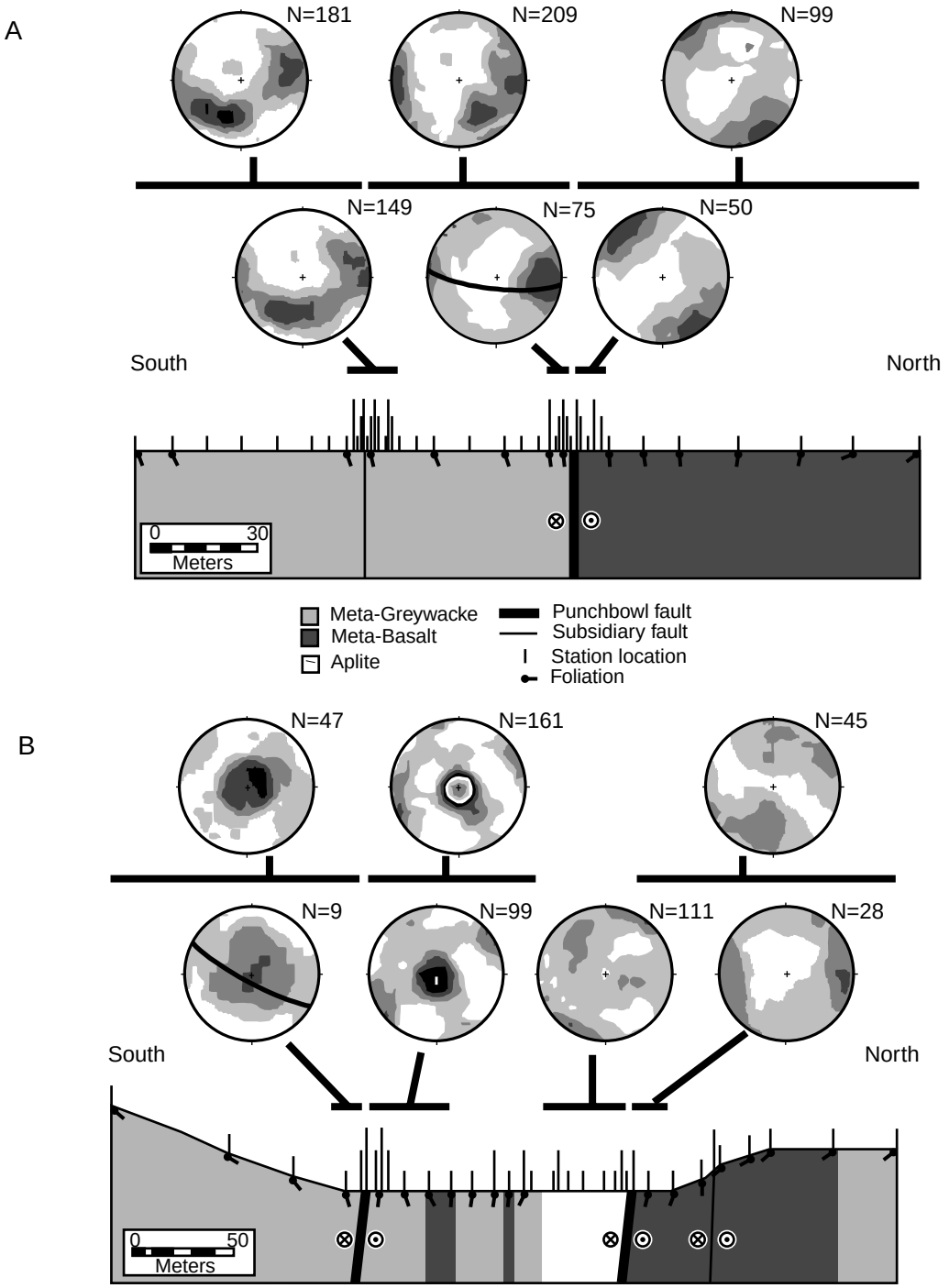

Fig. 2. Cross-sections of traverses. Subsidiary faults are large faults that do not appear to have as much associated deformation as the main branches of the Punchbowl Fault. Tadpoles indicate the apparent dip of the schistose foliation in the Pelona Schist. Lower hemispheric stereographic projections of fracture orientations are also shown. Mean orientation of the fault core is shown by the great circle in stereogram. The Kamb contour plots are of the density of the poles relative to the uniform population, with the first contour level at 3 sigma, and a contour interval of 2 sigma. Inverted 'T-bars' indicate stations from which stereonets are taken. Note differences in scales. (a) Cross-section and fracture date for traverse 1. (b) Cross-section and fracture orientation data from traverse 2. (c) Cross-section and fracture orientation data from traverse 3.

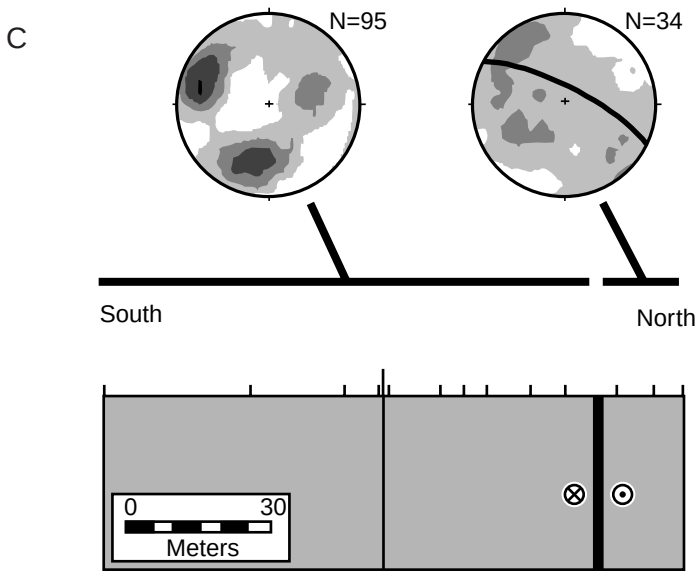

Fig. 2 (*continued*)

verse 3 is oriented N 50° E, and makes an angle of ~70° with the trend of the fault. Thus, in all cases, the Terzaghi correction for faults and fractures subparallel to the main trace of the Punchbowl Fault is small. Conversely, the planar structures, which formed at high angles to the fault, are undersampled. Local, meter-scale irregularities of the outcrop enable some of this undersampling to be corrected. We also show below that some of our results regarding fault-normal fractures would be made even more conclusive by applying a Terzaghi correction to these fractures.

3. Results

3.1. Methodology

We quantify the amount of brittle fault-related deformation along each traverse (Fig. 2). Stations at selected points along each traverse begin from the outer edge of the fault core and extend through the damaged zone and fault core. Previous studies of the San Gabriel and Punchbowl Faults (Chester and Logan, 1986; Chester et al., 1993; Evans and Chester, 1995) show that much of the deformation associated with large strike-slip faults in this area formed well within 100 m of the fault core. Chester et al. (1993) and Evans and Chester (1995) noted that the density of the brittle structures associated with the Punchbowl and San Gabriel Faults is localized within 10 m of the fault cores. Because of the expected concentration of structures close to the fault cores, we use a logarithmic sampling approach to data collection. Exposure permitting, stations along the traverses were placed every meter for the first 10 m from the fault core, then on every 10 m beyond the fault core. When there was no exposure at one of these predetermined locations, the nearest outcrop was used. In a few instances, the outcrops are too weathered to provide a reliable measure of fault-related deformation.

We used a line intersection (Hudson and Priest, 1983) inventory method at each station to measure the numbered orientations of small faults, fractures, and veins and to measure foliation orientation. Samples for thin sections were also collected at each station. Two vertical and two horizontal 70-cm-long scan lines were used at each station, to reduce the effect of local variations in each outcrop on the results.

We use one-dimensional scan-line methods (c.f. Hudson and Priest, 1983) rather than two-dimensional or fractal methods (La Pointe, 1988; Gillespie et al., 1993) because the exposures have limited vertical extents of 5–10 m. We span three orders of magnitude in our scales of observation (millimeter and centimeter scale, Schulz and Evans, 1998, to the meter-scale in this paper) and we make some comparisons between these scans of observation in our discussion of the results. The data from the two vertical transects were averaged, added to the average of the two horizontal transects to determine the number of damage elements, and plotted in relation to the distance from the fault core. All orientations are plotted separately. The vein density is highly variable and was analyzed separately from the other damage elements, and fractures are denoted in the field as surfaces along which there is no evidence of slip.

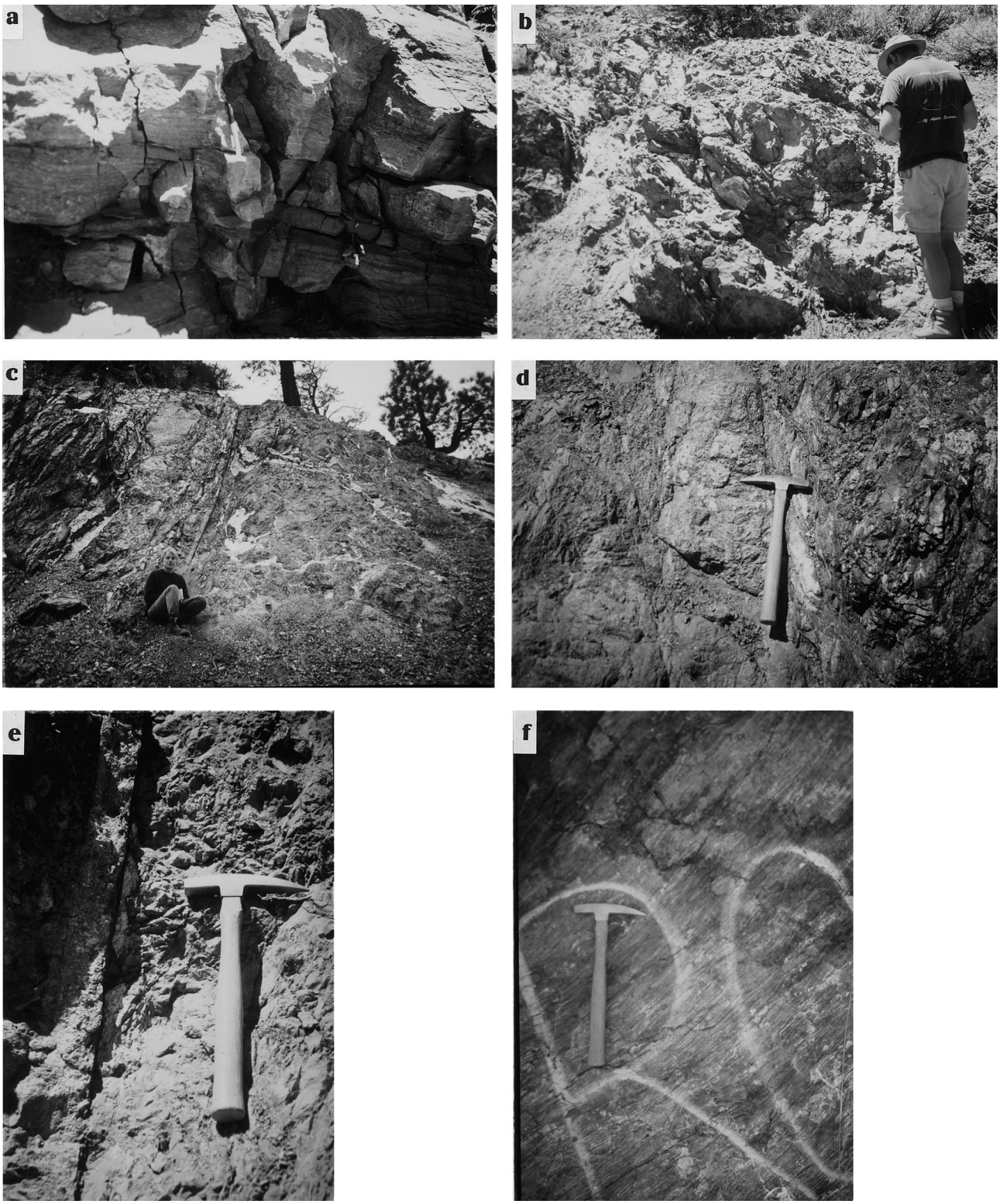

Fig. 3. Outcrops of the Pelona Schist near the Punchbowl Fault. (a) Pelona Schist 80 m north of the Punchbowl Fault at traverse 1. The schist is undeformed, with little fracturing along the foliation. (b) Exposure 47 m north of the Punchbowl Fault at traverse 1. The schist is more deformed, with increased fracturing along and across foliation. (c) The north branch of the Punchbowl Fault, traverse 1. The trace of the Punchboal Fault is seen as a sub-vertical dark line to the right of the seated figure with the view toward the northwest. Note the damaged rock north of the fault trace exhibits little foliation and numerous light veins in the greenschist. Grayschist south of the fault trace displays a prominent foliation that is sub-parallel to the fault. (d) Pelona Schist 5 m south of the southern fault core of the Punchbowl Fault at traverse 3. The rock is highly deformed and heavily altered. (e) Close-up view of the main trace of the fault at traverse 2. A 15-cm-thick breccia zone is located south of the fault core, 1-cm-thick slip surface is the dark, sub-vertical band cutting the rock. (f) Undeformed Pelona Schist 100 m south of the fault core, traverse 3. Lettering on rock is graffiti.

3.2. Qualitative descriptions of fault-related rocks

We first offer general descriptions of the rocks in outcrop to provide a general framework of the fault zone. Undeformed rocks are those for which schistosity is easily recognized, and fracture spacing is ~0.5–1 m. Alteration at the outcrop was noted by the presence of white–grey, chalky vein fillings, fracture linings, and replacement clay feldspar-rich folia. This zeolite-rich alteration (Schulz and Evans, 1998) is rare in the host rocks.

The schist in traverse 1 is relatively undeformed up to roughly 30 m from the fault trace, where the rock changes from a thinly foliated, grey, quartz–mica schist to a green–grey, highly fractured altered rock (Fig. 3a). The schist has a well-defined foliation north of the fault core and its orientation is unaffected by the Punchbowl Fault. Beginning at 30 m north of the fault core, foliation is difficult to distinguish (Fig. 3b). Within 8 m of the fault core, the rocks are extremely fractured and friable (Fig. 3c). South of the fault core at traverse 1, between the two branches of the Punchbowl Fault, the rocks are green–brown altered schists where fractures and slip surfaces are prevalent.

The fault core at all locations in this study is dark, fine grained and foliated to massive cataclasite. The fault core of the north branch of the Punchbowl Fault at traverse 1 is less than 10 cm thick, with a brecciated zone roughly 15 cm thick on the south side of the fault core that is continuous across much of the outcrop (Fig. 3d). This breccia zone is parallel to foliation but truncated by the fault core. The foliation surfaces are subparallel to the fault core, and they commonly contain slickenlines that plunge within 20° of horizontal.

Along traverse 2, the schist exhibits widely spaced (20 cm apart) fractures at greater than 60 m north of the fault core. At 15 m north of the fault core, fracture spacing is typically 2–5 cm and contains many more slip surfaces and veins than at 60+ m. Between the two branches of the Punchbowl Fault, the amount of alteration and deformation is irregular.

Rocks at traverse 3 are grey schists which are little altered beyond 15 m from the fault core (Fig. 3e). Within 15 m of the fault core, the rocks are much more altered. The rocks within 5 m of the fault core have little recognizable foliation and are very friable (Fig. 3f). There is also an increase in the density of slip surfaces close to the fault core, as well as locally abundant veins.

The fault core of the southern branch of the Punchbowl Fault at traverse 3 consists of a group of anastomosing gouge and cataclasite layers. Typically the gouge layers are bounded by slip planes that usually show distinct slickenlines indicating strike-slip motion (less than 10° from horizontal). The rock surrounding

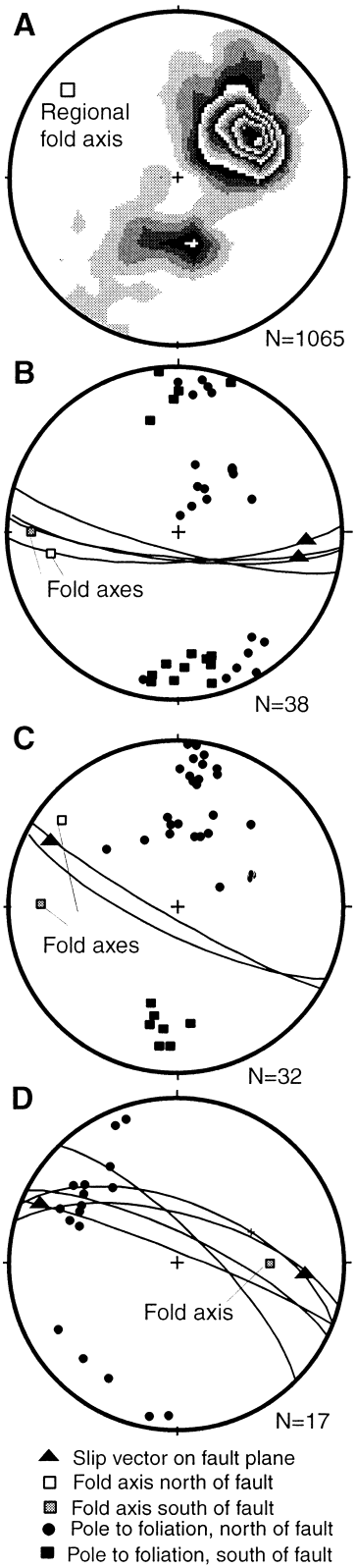

Fig. 4. Lower hemispheric stereographic projections of the fault core orientations, slip vectors, poles to foliation, and fold axes at the three traverses. Slip vectors, which are included for slip surfaces where they were obtainable, show that the slip sense is right-lateral. (a) Regional fold axis data for Pelona Schist. (b) Data for traverse 1. (c) Data for traverse 2. (d) Data for traverse 3.

the gouge layers is fine grained, friable, and locally foliated or brecciated. The rocks more than 10 m north of the fault core have a schistose foliation and are less deformed than the rock adjacent to the core, although they show a much greater abundance of fractures and slip surfaces than the undeformed host rock south of the fault core.

These qualitative observations of the rocks suggest that the majority of the deformation associated with the Punchbowl Fault occurs within 50 m of the fault core, with the most intense alteration and deformation concentrated within roughly 15 m of the fault core.

3.3. Structural analysis

As determined at the outcrop scale, the orientations of the fault cores vary among the three traverses (Fig. 4). The fault cores all dip steeply, ranging from 80°S to 79°N, with slickenlines that plunge approximately 20° (Fig. 4). We determine the intensity of deformation from the reorientation of schistosity, the densities of fractures and faults, and vein densities.

3.3.1. Reorientation of schistosity

Deformation of pre-existing structures is one method of estimating fault-zone thickness and strain distribution adjacent to a fault (c.f. Chester et al., 1993). In this study, the foliation of the Pelona Schist provides a regional marker to determine the fault on the protolith. We can do this because the Pelona Schist is broadly arched such that schistosity strikes NW–SE over the entire region (Jacobson, 1980, 1983a). Isoclinal folding of the schist (Jacobson, 1983a,b) produced NW-trending fold axes, which do not coincide with the form nor orientation of fold axes derived here.

The dip of the foliation steepens near the fault at all three traverses (Fig. 4). At traverse 1, the dip of the foliation steepens from 0–50° to 90° and to overturned at roughly 50 m north of the fault core and remains close to vertical throughout the damaged zone. The foliation dip is also nearly vertical between the two strands of the Punchbowl Fault. The strike of the foliation is rotated roughly 45°, becoming subparallel to the north branch of the Punchbowl Fault within 50 m of the fault core along traverse 1 (Fig. 4b). In between the two branches, the foliation orientation is subparallel to the fault core.

In traverse 2, the foliation 100 m from either side of the Punchbowl Fault dips shallowly and coincides with the regional orientation (Fig. 4c). The foliation steepens by 40° to nearly vertical within 50 m of the northern fault core and by 30° within 20 m of the southern fault core. Between the two branches of the Punchbowl Fault, the foliation ranges in dip from 73° to vertical, with the strike subparallel to the fault core. The strike rotation along traverse 2 is greater than 30°. The schistose foliation between the two strands has more variation in orientation than in traverse 1, with local folding near the southern fault core.

At traverse 3, a reorientation in the strike of the schistose foliation of almost 90° occurs within 10 m of the south trace of the Punchbowl Fault (Fig. 4d). North of the fault core the foliation is subparallel to the main trace of the Punchbowl Fault over a distance of at least 20 m. The dip of the foliation steepens by roughly 30° near the fault. The reorientation of foliation occurs much closer to the fault core at traverse 3 than in the other two traverses.

The data show that the foliation is reoriented subparallel to the main trace of the Punchbowl Fault over a zone no more than 50 m from the fault core. The changes in the strike of the foliation are not as dramatic as the changes in dip. In all cases, the foliation steepens adjacent to the Punchbowl Fault.

Fold axes derived from the schistosity all fall on or near the fault zone (Fig. 4). The folds are cylindrical, and fold axes are subparallel to the slip vectors (Fig. 4). Similar to more ductily deformed rocks (Bryant and Reid, 1969; Escher and Watterson, 1974; Hobbs et al, 1976, pp. 286–287), these data suggest that the folding which caused foliation reorientation may be the result of frictional drag on the Punchbowl Fault or rotation due to simple shear in the fault zone. It appears that slip on the Punchbowl Fault resulted in up to 50–60° of rotation of schistosity. Once the foliation was rotated parallel to the fault, no further rotation may have occurred because further slip could have been taken up along foliation surfaces. The crudely defined motion path of the fold axes suggests that the fault zone is a zone of simple shear with a component of thinning (Jiang and Williams, 1999). The mesoscopic mechanisms for folding were probably brittle slip on fault and fracture surfaces in the damaged zone, which exhibits numerous orientations of faults and fractures.

3.3.2. Fracture orientations

The orientations and densities of small faults and fractures help provide constraints on the structure of faults. These data can be used to infer the orientations of stresses near the faults (Chester et al., 1993). In our study, however, we cannot establish if the fractures are shear or extensional in origin, nor when they formed during the evolution of the fault zone, making it difficult to use them as paleostress indicators.

At traverse 1, the main fault trace strikes 096° and dips 80°SW. North of the fault core fractures strike ~060° and dip steeply to vertical (Fig. 2a). This orientation persists even close to the fault core. Within the fault zone traverse 1 fracture orientations exhibit a girdle pattern (Fig. 2a), south of the fault core the frac-

tures strike nearly due north and dip steeply. The girdle pattern continues southward into the protolith (Fig. 2a).

The south branch of the Punchbowl Fault at traverse 2 strikes 120° and dips 84°SW (Fig. 2b). North of the northern branch of the fault at traverse 2, little preferred orientation of fractures exists. There is a strong clustering of subhorizontal fractures between the two branches of the Punchbowl Fault (Fig. 2b), although no preferred orientation of fractures exists in the aplite between the two fault branches. South of the southern branch at traverse 2, the fractures are oriented similarly to those fractures between the two branches (Fig. 2b). Close to the fault core there are

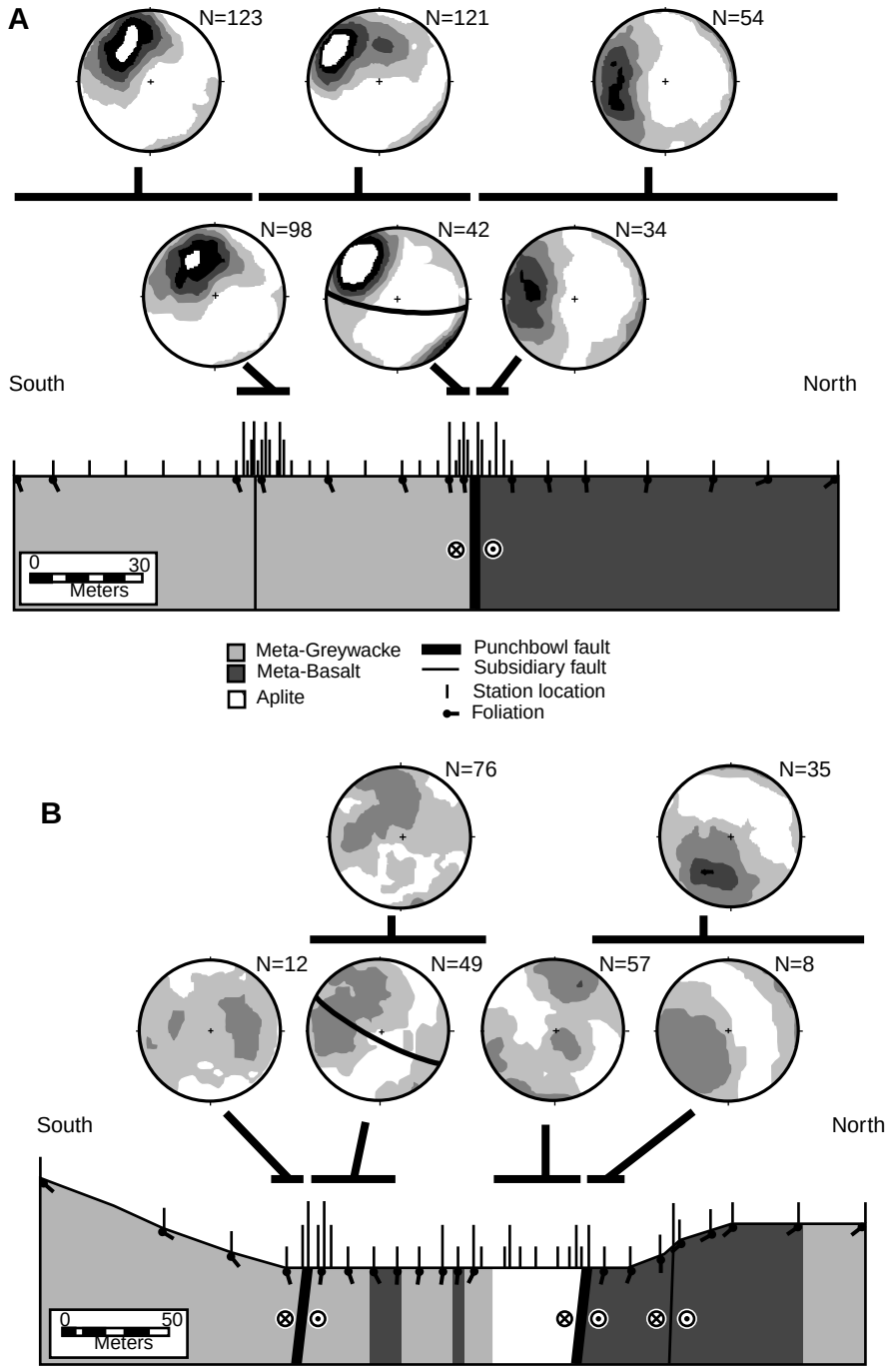

Fig. 5. Lower hemispheric stereographic projections of slip surface orientations along each traverse. The mean orientation of the fault core is shown by the great circle. The Kamb contour plots are of the density of the poles relative to a uniform population, with the first contour level at 3 sigma, and a contour interval of 2 sigma. Inverted 'T-bars' indicate stations from which stereonets are taken. (a) Data for traverse 1. (b) Data for traverse 2. (c) Data for traverse 3.

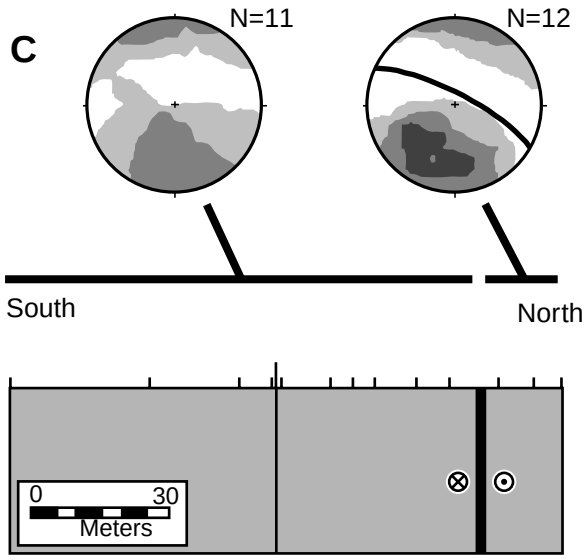

Fig. 5 (*continued*)

too few data points to define the geometries of the damage elements.

The south branch of the Punchbowl Fault at traverse 3 strikes 297° and dips 75°NE. Two main concentrations of fracture orientations occur south of the fault at traverse 3 (Fig. 2c). This is similar to the girdle distribution seen in the intrafault damaged zone at traverse 1 (Fig. 2a), although there is a significant scatter to the data. North of the fault, the fracture orientations are scattered. In summary the fracture orientation data show that orientations vary from traverse to traverse, but many fractures are at high angles to the fault.

3.3.3. Small fault data

Small faults in the study area are often difficult to recognize, as the Pelona Schist in much of the area does not contain well-developed marker units. Small faults were recognized by the presence of slickenlines, although determining a slip sense was difficult. North of the fault core at traverse 1 the slip surface orientations are clustered, although not as strongly as those south of the fault core (Fig. 5a). These small faults strike 347° and dip 48°E on average, with a high degree of scatter in the data. There is a distinct clustering of slip surfaces at high angles to the fault core in the rocks south of the north branch of the Punchbowl Fault at traverse 1 (Fig. 5a), with a mean strike of 054° and dip of 43°SE. This clustering about a NE strike continues to the southwest of the south branch. This orientation may reflect the kinematics of the brittle faults as seen in both field and laboratory experiments (Logan et al., 1981; Petit, 1987), as they could be P shears of a Riedel shear system (Logan et al., 1981).

The slip surface data for traverse 2 (Fig. 5b) are not as strongly clustered as the data for traverse 1. North of the north strand of the Punchbowl Fault, small faults strike 294° and dip 39°NE on average, which is close to the strike of the main fault although the dips differ by 60° (Fig. 5b). Between the two main fault traces, the orientations are varied.

At traverse 3 (Fig. 5c), most of the small faults dip moderately to steeply north or northeast, and there is no significant difference between the orientations of small faults on either side of the southern strand of the Punchbowl Fault. Only a small number of faults were measured at traverse 3, making conclusions drawn from these data speculative.

A detailed kinematic or pseudo-dynamic analysis of the small fault data is not warranted, as we do not have clear timing constraints for the development of the small faults. The pseudo-focal mechanism analysis (Angelier and Mechler, 1977; Lisle, 1987), using the technique of Allmendinger et al. (1992), shows the possible limitations of such analyses (Fig. 6). For both traverse 1 and 2, inversion of the small faults shows two possible nodal planes: a steeply dipping, east–west striking, left-lateral strike-slip fault, or a shallowly dipping, N- or NE-striking, right-lateral strike-slip fault. Both are clearly at odds with the right-lateral slip of the steeply dipping Punchbowl Fault, and suggest either: (a) the faults experienced significant rotation after formation, or (b) an early and complete mechanical separation between slip on the damaged zone and slip on the fault core. The latter was suggested by Chester et al. (1993) for the North Branch of the San Gab-

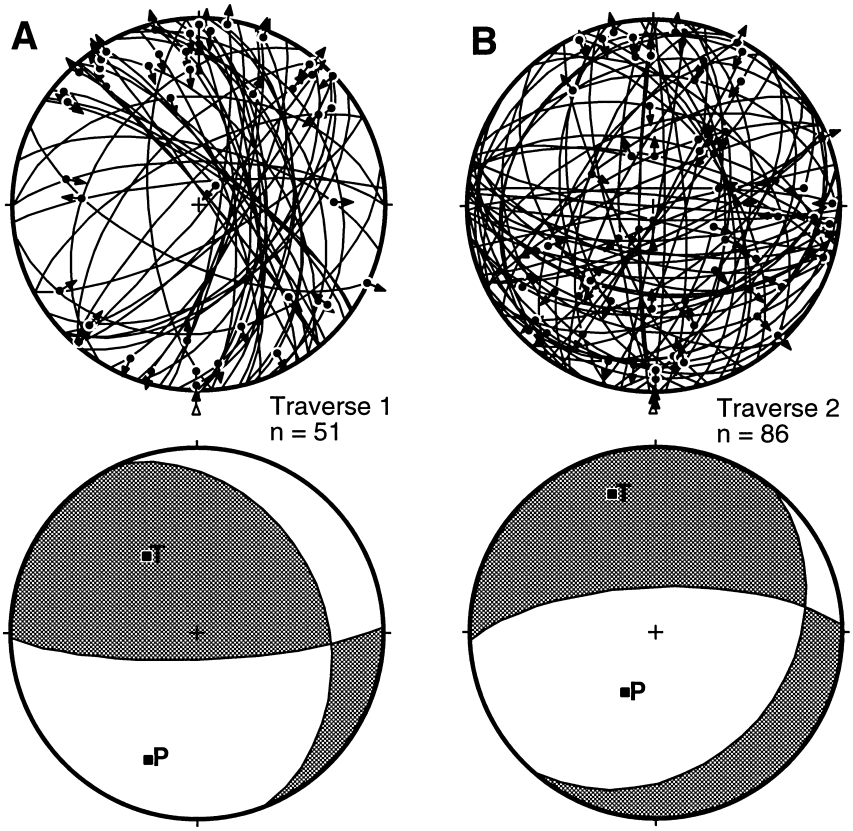

Fig. 6. Pseudo-focal mechanism solutions for the subsidiary faults along the traverses. Nodal planes are computed using the software of Allmendinger et al. (1992). Both traverses yield one nodal plane, which has approximately the same orientation as the Punchbowl Fault, but a left-lateral sense of slip. (a) Pseudo-focal mechanism solution and data for Traverse 1. (b) Pseudo-focal mechanism solution and data for Traverse 2.

riel Fault and has been observed in other seismogenic faults (Ito et al., 1998; Ohtani, et al., in press).

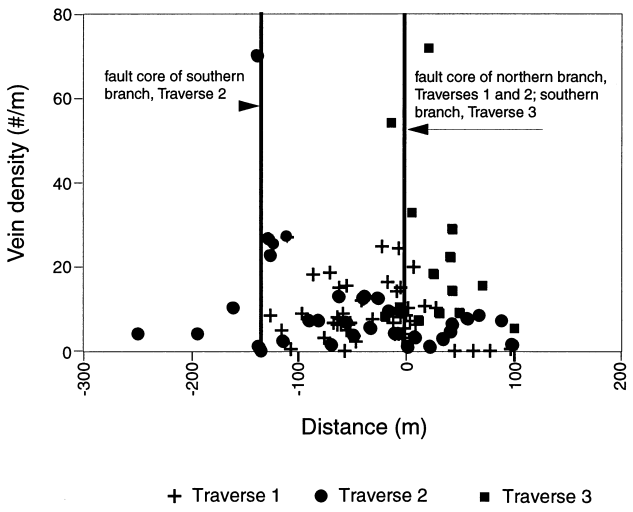

Fig. 7. Spatial distribution of mesoscopic veins along the three traverses. The distance of 0 m is the north branch of the Punchbowl Fault at traverse 1 and 2 and the south branch at traverse 3. All of the negative distances are between branches of the fault, except for traverse 2. The southern branch at traverse 2 is located at 133 m, so everything beyond this point is outside of and south of the fault.

3.3.4. Vein density

Veins in the study area are thin, mainly filled with quartz, calcite, and minor laumontite, and 5–100 cm long. Whereas there appears to be a general increase in vein density close to the fault cores (Fig. 7), the locations of increased vein density are scattered and do not follow the trends seen in the other deformation structures, especially in traverse 2.

In traverse 1, veins become abundant 20 m from the fault core; at distances greater than 20 m north of the core, veins are nearly absent. The number of veins south of the fault core at traverse 1 is highly variable, ranging from 0 to greater than 201 m. North of the fault core of traverse 2, the vein densities are sporadic, and do not increase close to the core. Between the two fault cores, the vein densities vary similarly to what is seen at traverse 1. The greatest vein density in traverse 2 occurs at the southern fault core. In traverse 3, there is a general increase in vein densities close to the fault core, but as in the other traverses, there is a large variability in the data.

We might anticipate an increase in vein density near the fault core, and we attribute the absence of higher densities to the destruction of veins by subsequent slip. This process is supported by the microstructural obser-

vations of the Punchbowl Fault (Schulz and Evans, 1998) and of the observations of the San Gabriel Fault (Chester et al., 1993).

3.3.5. Total damage intensity

The increase in the density of damage elements begins roughly 50–70 m from the fault core at both long traverses (Fig. 8a and b). The rocks near the fault core show a damage element density about 10 times greater than that of the rocks 100 m from the fault core for traverse 1, and four times greater for traverse 2. The rocks directly south of the fault core at traverse

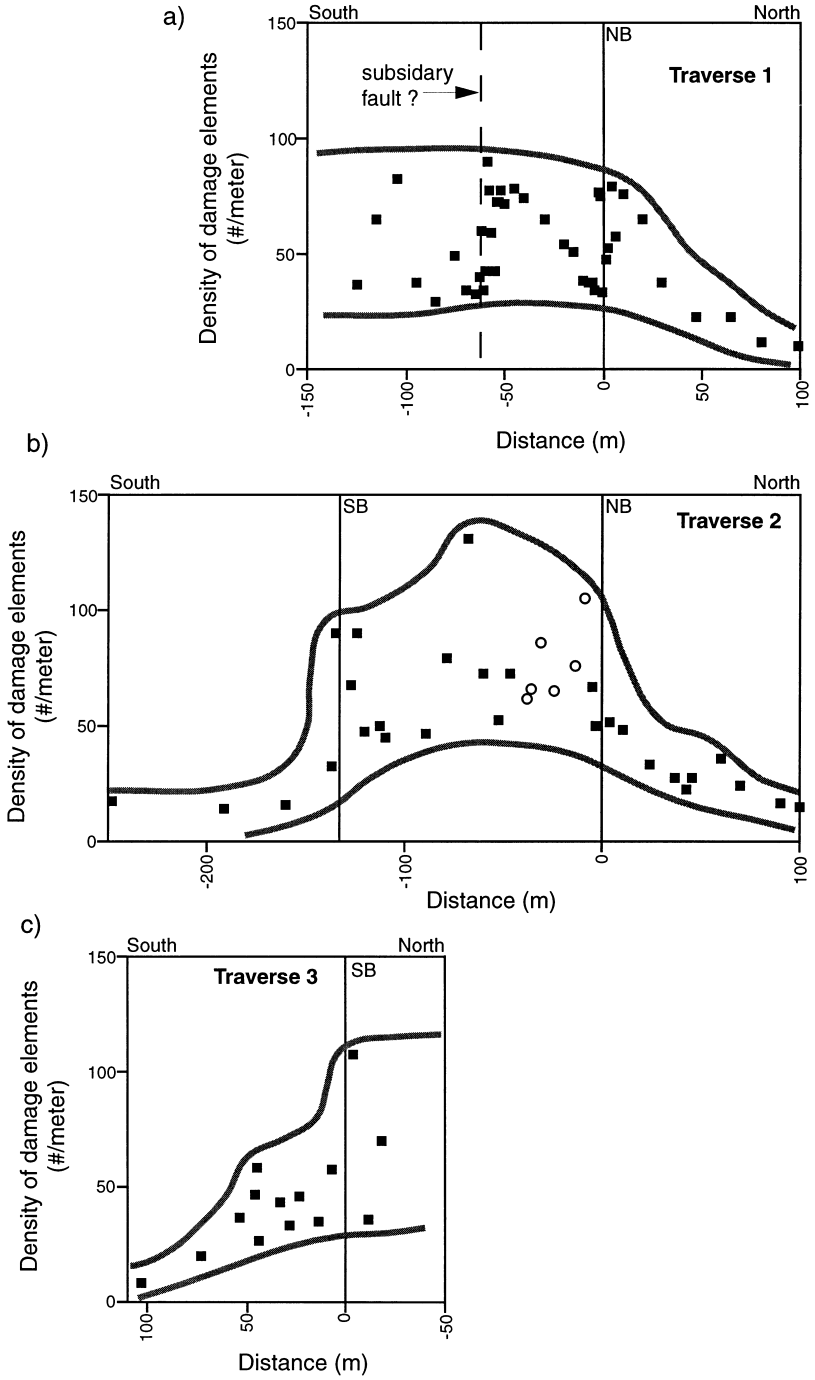

Fig. 8. Densities of mesoscopic damage elements plotted with respect to the distance from the fault core. Open circles are in aplite and closed squares in the Pelona Schist. Solid lines indicate the location of fault cores of the major strands of the Punchbowl Fault. Subsidiary faults are indicated by dashed lines. Grey lines outline the maximum and minimum deformation ranges measured. (a) Traverse l. (b) Traverse 2. (c) Traverse 3.

1 show an apparent decrease in the number of damage elements. However, a second peak in the density of damage elements occurs 55 m south of the fault core and corresponds to a subsidiary fault (Fig. 8a). This local increase in the density of damage elements is possibly an indication of slip localization within the fault zone. The density of damage elements between the two strands of the Punchbowl Fault is variable, but it is always greater than the density in the undeformed protolith. The highest density of damage elements within the intrafault damaged zone occurs within 10 m of the fault core.

For traverse 2, a small increase in the deformation density 60 m north of the northern fault core is associated with a subsidiary fault (Fig. 8b). South of the southern branch of the Punchbowl Fault, the increase in deformation within the damaged zone appears to begin closer to the fault core than that which is seen north of the fault. However, with the limited exposure south of the Punchbowl Fault, it is difficult to determine the protolith-damaged zone contact with much certainty.

At traverse 3, the macroscopic density of damage elements in the damaged zone is lower than at the other two traverses (Fig. 8c). The deformation associated with the Punchbowl Fault begins to increase at about 50 m from the fault core. A small increase in the density of damage elements 45 m south of the fault core corresponds to a subsidiary fault. The density of damage elements south of the fault core is variable but generally greater than that in the undamaged protolith.

The mesoscopic analysis shows that the deformation associated with the Punchbowl Fault increases from the relatively undeformed protolith to maximum levels at the regions of slip localization. For all three traverses, the increase in the density of damage elements begins 50–70 m from the fault core. Fractures, faults, and veins become pronounced roughly 20 m from the fault core. The density of damage elements between the two branches of the Punchbowl Fault shows a large amount of variability in both traverses 1 and 2, but is generally lower than the densities at the fault core and greater than the density of the undeformed rock over 50 m north of the fault core. The density data may under-represent the actual amount of macroscopic deformation, as the schistose foliation masks fractures and slip surfaces in the Pelona Schist.

4. Discussion

We discuss our results from two viewpoints. First we describe the implications of our work for the structural analysis and evolution of faults, and we conclude with some remarks regarding geophysical imaging of faults, the implications for seismic energy radiation, and for drilling into active faults.

4.1. Structural implications

Our results, and recent work of others (Ito et al., 1999; Ohtani et al., in press) show that the thickness of a given fault zone depends upon the type of deformation used to describe it, as well as the scale of observation (Fig. 9). Mesoscopic fractures and small faults examined in this study suggest that the fault zone begins between 50 and 70 m from the fault core, whereas the onset of fault-related microfracturing occurs at approximately 40 m from the fault core.

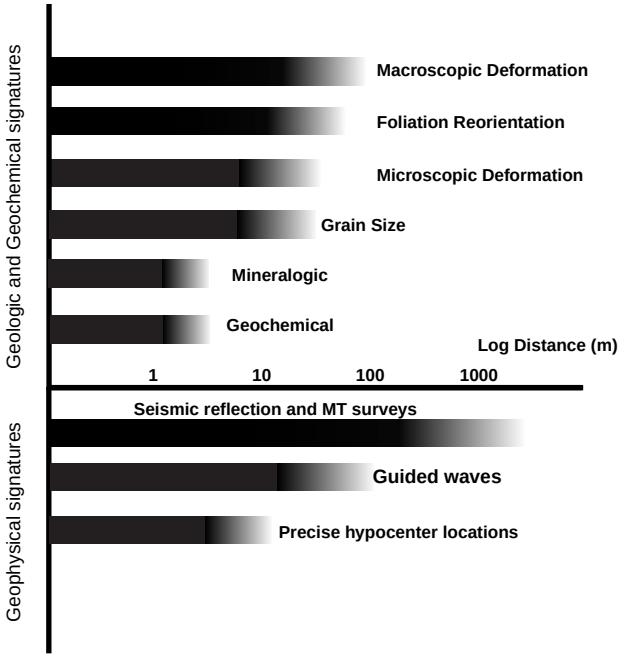

Fig. 9. Summary of spatial variability in the extent of fault-related deformation, alteration, and geophysical signature of major strike-slip faults. The bars indicate that the half thickness of the fault zone is measured from the center of the fault core into the undeformed protolith. The ends of the bars fade out because it is difficult to determine the exact point that the fault zone begins. Dashed line represents the location of the fault core. Approximate extent of mesoscopic, microscopic, and geochemical fault zone-related deformation and alteration over approximately 100 m. Data are combined from this paper and Schulz and Evans (1998). The lower graph shows the approximate extent of fault zone-related deformation and geophysical imaging of fault zones over approximately 1000 m. Seismic reflection and MT data for various strike-slip faults (Feng and McEvilly, 1983; Mogi et al., 1991; Eberhart-Phillips et al., 1995; Unsworth et al., 1997; Stern and McBride, 1998). Mesoscopic and microscopic deformation widths taken from Chester et al. (1993), this paper, and Schulz and Evans (1998). Guided waves from Li et al. (1990), Li et al. (1994a,b, 1998), Ben-Zion (1998). Hypocenter locations from Nadeau et al. (1995), Eberhart-Phillips and Michael (1993). Geochemical width from Evans and Chester (1995), Schulz and Evans (1998).

Reorientation of pre-existing foliation occurs over a zone 30 m wide. Geochemical data suggest a thickness of less than 10 m, grain-size reduction occurs over a 10-m-wide region, and significant mineralogic changes occur over a region 20–30 m wide (Schulz and Evans, 1998).

Three traverses across the Punchbowl Fault show that the damaged zone is present on both sides of the fault core, with an increase in meso- and microscopic damage element densities close to the fault core and the greatest intensity adjacent to the fault core. The damaged zone thickness is not the same on both sides of the fault core in either spatial extent or amount of deformation. Traverse 2 shows that the southern damaged zone is not as thick and is less deformed than the damaged zone on the north side of the Punchbowl Fault.

The majority of the differences between the fault zone studied here and those examined by others (Chester and Logan, 1987; Chester et al., 1993; Evans and Chester, 1995) appear to be within the damaged zone. The damaged zone of the Punchbowl Fault in sedimentary rock is thinner (by approximately 15 m) than that in the Pelona Schist, although the zone varies in thickness along strike (Chester and Logan, 1986). The damaged zone of the San Gabriel Fault is wider, roughly 200 m thick, with the primary deformation being cataclasis (Chester et al., 1993). Thus it appears that the layered rocks produce a thinner damaged zone.

Where the Punchbowl Fault has multiple fault cores, each has its own damaged zone. In much of the study region, these cores are separated by as much as 1.2 km, although in the eastern portion, the multiple fault cores are closely spaced anastomosing features. The damaged zone rocks between two fault cores are more deformed and altered than those on the outer sides of the fault cores, implying that the damaged zones overlap. Smaller faults within the zone between the two major branches are also sites of slip localization, and they create their own concentrations of deformation. The 'intrafault' damaged zone is similar to the damaged zone outside of, but close to, the main branches, in both the type and amount of deformation present.

These data suggest that some portions of the SAF system may consist of multiple slip surfaces embedded within overlapping damaged zones that are regions of enhanced microfracturing, alteration, and reorientation of primary structures. A distinct mechanical and hydrologic partitioning may thus be the norm for the fault zones of depth. Curewitz and Karson (1997) suggest that the mechanical interaction of propagating faults may lead to enhanced fracture densities adjacent to the faults. We do not have timing constraints on the two strands of the Punchbowl Fault, but the increased amount of damage between the fault strands may be the result of such dynamic interactions. Alteration of the host rock is prevalent throughout the entire 'intrafault' damaged zone at traverse 1 but not at traverse 2, showing that there is along-strike variation in the amount of 'intrafault' alteration.

Veins associated with the Punchbowl Fault are scattered throughout the damaged zone with no apparent relationship to the distance from the fault core; they do not display the increase in density close to the fault core that has been documented along other large faults. This indicates a different fluid–rock interaction in portions of the fault zone and may suggest that fluids were not concentrated close to the fault core (see Schulz and Evans, 1998). Alternatively, this may suggest that the composition of the fluids varies within the fault. The widely distributed region of veins may suggest a wider region of permeability, as compared to the extremely vein-rich damaged zone documented by Chester et al. (1993).

The presence of a damaged zone which consists of interconnected fractures adjacent to the principal slip surface(s) might make it difficult for pore fluid pressures to build up beyond hydrostatic, thereby making it difficult to invoke models of high pore fluid pressure for faulting (e.g. Byerlee, 1990; Rice, 1992; Byerlee, 1993). Rapid sealing (Blanpied et al., 1992) by vein development may create seals in the damaged zone (Chester et al., 1993).

4.2. Seismological/geophysical implications

A variety of geophysical methods have been employed to image the San Andreas and related faults, as well as several other large-displacement strike-slip faults, and these data also indicate that fault zone width varies as a function of the technique used to image the fault (Fig. 9). Seismic reflection studies (Feng and McEvilly, 1983; Stern and McBride, 1998), velocity models (McCaffree-Pellerin and Christensen, 1998), magnetotelluric studies, (Mogi et al., 1991; Unsworth et al., 1997), and tomographic studies (Michelini and McEvilly, 1991; Eberhart-Phillips and Michael, 1993; Scott et al., 1994) suggest that some major strike-slip faults consist of a low-velocity zone (LVZ) as thick as 2–3 km. Fault-guided waves have been used to infer fault zone widths of ~100–200 m for the SAF (Li and Leary, 1990; Ben-Zion and Malin, 1991; Li et al., 1994a,b, 1997a; Ben-Zion, 1998) and the San Jacinto Fault (Li et al., 1997b), a width of ~30–60 m for the Nojima Fault (Li et al., 1998) and smaller faults (Hough et al., 1994; Lou et al., 1997). Precisely located earthquakes (Eberhart-Phillips and Michael, 1993; Nadeau et al., 1995; Rubin et al., 1999) typically define a very narrow (< 200 m, and in some cases, < 20 m wide) plane of hypocenters. Analysis of after-

shocks can show a dichotomy between the kinematics of the main slip surface and the rocks adjacent to the fault zone (Oppenheimer et al., 1988), suggesting that a damaged zone not kinematically coordinated with the main fault forms during and after some earthquakes.

When reconciled with geophysical results (Fig. 9), our work indicates that many types of geophysical imaging use waveforms that are 'tuned' to the size of the damaged zone, in which the higher concentration of fractures, faults, and veins results in a zone of lower velocity relative to the protolith and a zone that would probably exhibit a different MT and velocity signature than the surrounding rock (see also Eberhart-Phillips et al., 1995; Stern and McBride, 1998). The damaged zone most probably has a reduced elastic modulus relative to the protolith (Bruhn et al., 1994) and higher fluid storativity (Caine and Forster, 1999). The damaged zone may also act as an effective wave-guide, especially in regions where the transition from the protolith and the damaged zone is sharp (Li and Vidale, 1996; Ben-Zion and Andrews, 1998). If large amounts of seismic energy are concentrated in the fault core, significant grain-size reduction and, where fluids are present, vein creation, destruction, and alteration would result in the fault cores. Energy dissipated into the damaged zones may result in the more diffuse nature of the distribution of faults, fractures, and alteration patterns observed there.

When reconciled with available geophysical data, the most reliable measure of the fault zone width is the density of micro- and mesoscopic deformation densities. Geochemical indicators are subject to the amount and composition of the fluids, the local and regional scale hydrogeologic setting, and possibly the time between earthquakes.

Not imaged with most geophysical techniques are the extremely narrow fault cores that accommodate most of the slip. These slip zones are likely to be extremely narrow and embedded within the imaged fault zone, and probably would go undetected by most methods. These fault cores must be sampled directly, either by drill-hole or field-based investigations, or by precisely locating hypocenters. Once linked, these fault cores may dominate the slip accumulation and strength of the fault and thus are important components of the fault.

Our data do not help explain what produces the very wide (2–3 km) LVZ often described in seismic profiles (Feng and McEvilly, 1983; Roure et al., 1989; Eberhart-Phillips et al., 1995; Eberhart-Phillips and Reyners, 1997; Stern and McBride, 1998; Zhao and Negishi, 1998). One possibility is that such zones consist of numerous principal slip surfaces with overlapping damaged zones. This suggests that future work on fault zone structure must also incorporate long traverses (up to 5 km) across major faults, in order to sample the fracture density and orientations. Such tests would help to constrain whether the wide LVZ, inferred from some studies, are artifacts of the limitations of the seismic methods, and if the trapped head waves are a more robust method for inferring the size of the LVZ.

Our results also have implications for the drilling and direct sampling of seismogenic faults. A thin central fault core surrounded by fractured and altered rock was encountered and successfully sampled in the Nojima Fault drill holes (Ando, 1997; Ito et al., 1998; H. Ito, personal communication, 1999). Other proposed attempts to retrieve cores from principal slip surfaces and to conduct borehole geophysics in other faulted regions dominated by crystalline rocks (e.g. Hickman et al., 1994, 1995) must be prepared for the possibility that the zone where slip is concentrated is extremely thin (~2–5 m) and surrounded by highly fractured and altered rocks.

5. Conclusions

The Punchbowl Fault, exhumed from a depth of up to 4 km, is composed of a macroscopically identifiable damaged zone, which surrounds thin core zones of localized slip. The apparent thickness of the fault zone varies with the parameter that is measured. Increased fracture densities are noted up to 70 m away from the fault core, whereas foliation reorientation occurs in a zone ~30 m wide. Microscopic and compositional changes occur over even narrower zones (Schulz and Evans, 1998). Damaged zones are associated with individual strands of the fault system, and overlapping damaged zones may form relatively wide regions of increased fracturing, alteration, grain-size reduction, and vein density.

Based on the distribution of microstructures, geochemical alteration, and changes in preexisting structures, the Punchbowl Fault zone is narrower where it cuts the schist than are other strike-slip faults developed in granitic gneisses (Chester et al., 1993). The data from the Punchbowl Fault show that the fault zone can be less than 200 m thick, with most of the deformation limited to an even thinner (20 m) zone of intense deformation and slip localization.

Acknowledgements

We thank Susanne Janecke and Don Fiesinger for reviews of a much earlier draft of this paper and to journal reviewers Bob Holdsworth and Diane Moore, whose comments helped us to improve the paper significantly. Collaboration and discussion with Fred

Chester, Jonathan Caine, and Zoe Shipton have been very helpful. Many thanks to Carl Jacobson for providing the regional foliation data for the Pelona Schist used in Fig. 4. Field assistance of Caleb Pollock is gratefully acknowledged. This work was funded by U.S.G.S. NEHRP Grants 1434-92-G2184 and 1434-94-G-2468, and NSF Grant EAR 9205774.

References

Allmendinger, R.W., Marrett, R.A., Cladouhos, T., 1992. Faultkin, A computer program for analysis of fault slip data.

Anderson, J.L., Osborne, R.H., Palmer, D.F., 1983. Cataclastic rocks of the San Gabriel Fault—an expression of deformation at deeper crustal levels in the San Andreas fault zone. Tectonophysics 98, 209–251.

Anderson, J.L., Osborne, R.H., Palmer, D.F., 1980. Petrogenesis of cataclastic rocks within the San Andreas fault zone of Southern California, USA. Tectonophysics 67, 221–249.

Ando, M., 1997. Geophysical and geological drilling into the Nojima fault; the 1995 Nyogoken–Nanbu earthquake fault in Awaji Island, Japan. EOS Transactions of the American Geophysical Union 78 (46 Suppl.), 492.

Angelier, J., Mechler, P., 1977. Sur une méthode graphique de recherche des contraintes principales égalment utilisable en tectonique et en seismologie: La méthode des dièdres droits. Bulletin Société Géologique de France 19, 1309–1318.

Ben-Zion, Y., Andrews, D.J., 1998. Properties and implications of dynamic rupture along a material interface. Bulletin of the Seismological Society of America 88, 1085–1094.

Ben-Zion, Y., 1998. Properties of seismic fault zone waves and their utility for imaging low velocity structures. Journal of Geophysical Research 103, 567–585.

Ben-Zion, Y., Malin, P., 1991. San Andreas Fault zone head waves near Parkfield, California. Science 251, 1592–1594.

Blanpied, M.L., Lockner, D.A., Byerlee, J.D., 1992. An earthquake mechanism based on rapid sealing of faults. Nature 358, 574–576.

Bruhn, R.L., Parry, W.T., Yonkee, W.A., Thompson, T., 1994. Fracturing and hydrothermal alteration in normal fault zones. Pure and Applied Geophysics 142, 609–644.

Bryant, B., Reid, Jr., 1969. Significance of lineations and minor folds near major thrust faults in the southern Appalachians and the British and Norwegian Caledonides. Geological Magazine 106, 412–429.

Byerlee, J., 1990. Friction, overpressure and fault normal compression. Geophysical Research Letters 17, 2109–2112.

Byerlee, J., 1993. Model for episodic flow of high-pressure water in fault zones before earthquakes. Geology 21, 303–306.

Caine, J.S., Evans, J.P., Forster, C.B., 1996. Fault zone architecture and permeability structure. Geology 24, 1025–1028.

Caine, J.S., Forster, C.B., 1999. Field-based numerical modeling of three-dimensional fault zone architecture, fracture networks, and fluid flow. In: Haneberg, W., Mozley, P.S., Moore, J.C., Goodwin, L.B. (Eds.), Impacts of Faults on Fluid Flow, 113. American Geophysical Union Monograph, pp. 101–128.

Chester, F.M., Logan, J.M., 1986. Implications for mechanical properties of brittle faults from observations of the Punchbowl Fault zone, California. Pure and Applied Geophysics 124, 79–106.

Chester, F.M., Logan, J.M., 1987. Composite planar fabric of gouge from the Punchbowl Fault, California. Journal of Structural Geology 9, 621–634.

Chester, F.M., Evans, J.P., Biegel, R.L., 1993. Internal structure and weakening mechanisms of the San Andreas fault. Journal of Geophysical Research 98, 771–786.

Curewitz, Dr., Karson, J.A., 1997. Structural settings of hydrothermal outflow: Fracture permeability maintained by fault propagation and interaction. Journal of Volcanology and Geothermal Research 79, 149–168.

Dibblee, T.W., 1968. Displacements on the San Andreas fault system in the San Gabriel, San Bernadino, and San Jacinto Mountains, Southern California. In: Dickinson, W.R., Grantz, A. (Eds.), Proceedings of the Conference on Geologic Problems of San Andreas Fault system, Geological Sciences, 11. Stanford University Publications, pp. 260–278.

Dibblee, T.W., 1987. Geology of the Devil's Punchbowl, Los Angeles County, California. Geological Society of America Centennial Field Guide Cordilleran Section, 207–210.

Eberhart-Phillips, D., Michael, A.J., 1993. Three-dimensional velocity structure, seismicity, and fault structure in the Parkfield region, Central California. Journal of Geophysical Research 98 (15), 737–758.

Eberhart-Phillips, D., Reyners, M., 1997. Continental subduction and three-dimensional crustal structure: the northern South Island, New Zealand. Journal of Geophysical Research 102, 11,843–11,861.

Eberhart-Phillips, D., Stanley, W.D., Rodriguez, B.D., Lutter, W.J., 1995. Surface seismic and electrical methods to detect fluids related to faulting. Journal of Geophysical Research 100, 919–936.

Ehlig, P.L., 1958. Geology of the Mt. Baldy region of the San Gabriel Mountains, California. Ph.D. Dissertation. University of California, Los Angeles, California.

Ehlig, P.L., 1981. Origin and tectonic history of the basement terrain of the San Gabriel Mountains, central Transverse Ranges. In: Ernst, W.G. (Ed.), The Geotectonic Development of California. Prentice-Hall, Englewood Cliffs, NJ, pp. 253–283.

Ehlig, P.L., 1987. Geologic structure near the Cajon Pass scientific drill hole. Geophysical Research Letters 15, 953–956.

Escher, A., Watterson, J., 1974. Stretching fabrics, folds, and crustal shortening. Tectonophysics 22, 223–231.

Evans, J.P., Chester, F.M., 1995. Fluid–rock interaction in faults of the San Andreas system: Inference from San Gabriel fault-rock geochemistry and microstructures. Journal of Geophysical Research 100, 7–20.

Evans, J.P., Forster, C.B., Goddard, J.V., 1997. Permeabilities of fault-related rocks and implications for fault-zone hydraulic structure. Journal of Structural Geology 19, 1393–1404.

Feng, R., McEvilly, T.V., 1983. Interpretation of seismic reflection profiling data for the structure of the San Andreas Fault Zone. Bulletin of the Seismological Society of America 73, 1701–1720.

Fisher, Q.J., Knipe, R.J., 1998. Fault sealing processes in siliciclastic sediments. In: Jones, G., Fisher, Q.J., Knipe, R.J. (Eds.), Faulting, fault sealing and fluid flow in hydrocarbon reservoirs, 147. Geological Society Special Publication, pp. 117–134.

Forster, C.B., Evans, J.P., 1991. Fluid flow in thrust faults and crystalline thrust sheets: Results of combined field and modeling studies. Geophysical Research Letters 18, 979–982.

Gillespie, P.A., Howard, C.B., Walsh, J.J., Watterson, J., 1993. Measurement and characterization of spatial distributions of fractures. Tectonophysics 226, 113–141.

Goddard, J., Evans, J.P., 1995. Chemical changes and fluid-rock interaction in faults of crystalline thrust sheets, northwestern Wyoming, U.S.A. Journal of Structural Geology 17, 533–547.

Guilbert, J.M., Park, C.F., 1985. The Geology of Ore Deposits. W. H. Freeman, New York.

Haneberg, W.C., 1995. Steady-state groundwater flow across idealized faults. Water Resources Research 31, 1815–1820.

Haxel, G.B., Budahn, J.R., Fries, T.L., King, B.W., White, L.D., Aruscavage, P.J., 1987. Geochemistry of the Orocopia schist, southeastern California: summary. In: Dickinson, W.R., Klute, M.A. (Eds.), Arizona Geological Society Digest, pp. 49–64.

Hickman, S.H., Zoback, M.D., Younker, L., Ellsworth, W., 1994.

Deep scientific drilling in the San Andreas fault zone. EOS, Transactions of the American Geophysical Union 75, 137–142.
Hickman, S.H., Younker, L.W., Zoback, M.D., Cooper, G.A., 1995. The San Andreas fault zone drilling project: Scientific objectives and technological objectives. Journal of Energy Resources Technology 117, 263–270.
Hobbs, B.W., Means, W.D., Williams, P.F., 1976. An Outline of Structural Geology. Wiley and Sons, New York.
Hough, S.E., Ben-Zion, Y., Leary, P., 1994. Fault-zone waves observed at the southern Joshua Tree earthquake rupture zone. Bulletin of the Seismological Society of America 84, 761–767.
Hudson, J.A., Priest, S.D., 1983. Discontinuity frequency in rock masses. International Journal of Rock Mechanics and Mining Sciences 20, 73–89.
Ito, H., Fujimoto, K., Ohtani, T., Tanaka, H., Higuchi, T., Tomida, N., Agar, S.M., 1998. Alteration and mass transfer along the GSJ borehole penetrating the Nojima earthquake fault. Annales Geophysicae 16 (Suppl. 1), 249.
Jacobson, C.E., 1983a. Structural Geology of the Pelona Schist and the Vincent Thrust, San Gabriel Mountains, California. Geological Society of America Bulletin 94, 753–767.
Jacobson, C.E., 1983b. Complex refolding of the Pelona, Orocopie, and Rand Schists, southern California. Geology 11, 583–586.
Jacobson, C.E., 1990. The 40Ar/39Ar geochronology of the Pelona Schist and related rocks, southern California. Journal of Geophysical Research 95, 509–528.
Jacobson, C.E., Dawson, M.R., Postlethwaite, C.E., 1988. Structure, metamorphism, and tectonic significance of the Pelona, Orocopia, and Rand Schists, southern California. In: Ernst, W.G. (Ed.), Metamorphism and Crustal Evolution of the Western United States, Rubey Volume, 7. Prentice-Hall, pp. 976–987.
Jiang, D., Williams, P.F., 1999. When do dragfolds develop into sheath folds in shear zones. Journal of Structural Geology 21, 577–584.
Li, Y., Aki, K., Adams, D., Hasemi, A., 1994a. Seismic guided waves trapped in the fault zone of the Landers, California, earthquake of 1992. Journal of Geophysical Research 99, 705–722.
Li, Y.G., Vidale, J.E., Aki, K., Marone, C.J., Lee, W.H.K., 1994b. Fine structure of the Landers fault zone: Segmentation and the rupture process. Science 256, 367–370.
Li, Y.G., Aki, K., Vidale, J.E., Alvarez, M.G., 1998. A delineation of the Nojima fault ruptured in the M7.2 Kobe, Japan, earthquake of 1995 using fault zone trapped waves. Journal of Geophysical Research 103, 7247–7263.
Li, Y.G., Leary, P.C., 1990. Fault zone trapped seismic waves. Bulletin of the Seismological Society of America 80, 1245–1271.
Li, Y.G., Vidale, J.E., 1996. Low-velocity fault zone guided waves: Numerical investigations of trapping efficiency. Bulletin of the Seismological Society of America 86, 371–378.
Li, Y.G., Ellsworth, W.L., Thurber, C.H., Malin, P.E., Aki, K., 1997a. Observations of fault-zone trapped waves excited by explosions at the San Andreas fault, central California. Bulletin of the Seismological Society of America 87, 210–221.
Li, Y.G., Vernon, F.L., Aki, K., 1997b. San Jacinto fault-zone guided waves: A discrimination for recently active fault strands near Anza, California. Journal of Geophysical Research 102, 689–701.
Lisle, R.J., 1987. Principal stress orientations from faults: an additional constraint. Annales Tectonicæ 1, 155–158.
Logan, J.M., Higgs, N.G., Friedman, M., 1981. Laboratory studies on natural gouge from the U.S. Geological Survey Dry Lake Valley No. 1 well, San Andreas fault zone. In: Carter, N.L., Friedman, M., Logan, J.M., Stearns, D.W. (Eds.), Mechanical Behavior of Crustal Rocks, The Handin Volume. American Geophysical Union, pp. 121–134.
Lopez, D.L., Smith, L., 1995. Fluid flow in fault zones: Analysis of the interplay of convective circulation and topographically driven groundwater flow. Water Resources Research 31, 1489–1503.
La Pointe, P.R., 1988. A method to characterize fracture density and connectivity through fractal geometry. International Journal of Rock Mechanics and Mining Sciences 25, 421–429.
Lou, M., Rial, J.A., Malin, P., 1997. Modeling fault zone guided waves of micro earthquakes in a geothermal reservoir. Geophysics 62, 1278–1284.
Matthai, S.K., Aydin, A., Pollard, D.D., Roberts, S.G., 1998. Numerical simulation of departures from radial drawdown in a faulted sandstone reservoir with joints and deformation bands. In: Jones, G., Fisher, Q.J., Knipe, R.J. (Eds.), Faulting, fault sealing and fluid flow in hydrocarbon reservoirs. Geological Society Special Publication, pp. 157–191.
McCaffree-Pellerin, C.L.M., Christensen, N.I., 1998. Interpretation of crustal seismic velocities in the San Gabriel–Mojave region, Southern California. Tectonophysics 286, 253–271.
Michelini, A., McEvilly, T.V., 1991. Seismological studies at Parkfield, I—Simultaneous inversion for velocity structure and hypocenters using cubic b-splines parameterization. Bulletin of the Seismological Society of America 81, 524–552.
Mogi, T., Katsura, I., Nishimura, S., 1991. Magnetotelluric survey of an active fault system in the northern part of the Kinki District, southwest Japan. Journal of Structural Geology 13, 235–246.
Nadeau, R.M., Foxall, W., McEvilly, T.V., 1995. Clustering and periodic recurrence of microearthquakes on the San Andreas fault at Parkfield, California. Science 267, 503–507.
Noble, L.F., 1954. The San Andreas fault zone from Soledad Pass to Cajon Pass, California. In: Jahns, R.H. (Ed.), Geology of Southern California, California Department of Resources, Division of Mines Bulletin, 170, pp. 37–48.
Oakshott, G.B., 1958. Geology and mineral deposits of San Fernando Quadrangle, Los Angeles County, California. California Division of Mines and Geology Bulletin, 172.
Ohtani, T., Fujimoto, K., Ito, H., Tanaka, H., Tomida, N., Higuchi, T., in press, Fault rocks and paleo- to recent fluid characteristics from the borehole survey of the Nojima fault ruptured in the 1995 Kobe earthquake, Japan, Journal of Geophysical Research.
Oppenheimer, D.H., Reasenberg, P.A., Simpson, R.W., 1988. Fault plane solutions for the 1984 Morgan Hill, California, earthquake sequence: Evidence for the state of stress on the Calaveras Fault. Journal of Geophysical Research 93, 9007–9026.
Petit, J.P., 1987. Criteria for the sense of movement on fault surfaces in brittle rocks. Journal of Structural Geology 9, 597–608.
Powell, R.E., 1993. Balanced palinspastic reconstruction of pre-late Cenozoic paleogeology, southern California: Geologic and kinematic constraints on evolution of the San Andreas fault system. In: Powell, R.E., Weldon II, R.J., Matti, J.C. (Eds.), The San Andreas fault system: Displacement, Palinspastic Reconstruction, and Geologic Evolution, 178. Geological Society of America Memoir, Boulder, Colorado, pp. 1–107.
Powell, R.E., Weldon R.J. Jr., 1992. Evolution of the San Andreas fault. Annual Review of Earth and Planetary Science 20, 431–468.
Rice, J.R., 1992. Fault stress states, pore pressure distributions, and the weakness of the San Andreas Fault. In: Evans, B., Wong, T.F. (Eds.), Fault Mechanics and Transport Properties Rocks. Academic Press, London, pp. 475–503.
Roure, F., Choukroune, P., Berastegui, X., Munoz, J.A., Villien, A., Matheron, P., Bareyt, M., Seguret, M., Camara, P., Deramond, J., 1989. ECORS deep seismic data and balanced cross sections: geometric constraints on the evolution of the Pyrenees. Tectonics 8, 41–50.
Rubin, A.M., Gilland, D., Got, J.-L., 1999. Streaking of microearthquakes along faults. Nature 400, 635–641.
Schulz, S.E., Evans, J.P., 1998. Spatial variability in microscopic de-

formation and composition of the Punchbowl fault, Southern California: implications for mechanisms, fluid–rock interaction, and fault morphology. Tectonophysics 295, 223–244.

Scott, J.S., Masters, T.G., Vernon, F.L., 1994. 3-D velocity structure of the San Jacinto fault zone near Anza, California; I, P waves. Geophysical Journal International 119, 611–626.

Sibson, R.H., Robert, F., Poulsen, K.H., 1988. High-angle reverse faults, fluid pressure cycling, and mesothermal quartz–gold deposits. Geology 16, 551–555.

Sibson, R.H., 1989. Earthquake faulting as a structural process. Journal of Structural Geology 11, 1–14.

Stern, T.A., McBride, J.H., 1998. Seismic exploration of continental strike-slip zones. Tectonophysics 286, 63–78.

Unsworth, M.J., Malin, P.E., Egbert, G.D., Booker, J.R., 1997. Internal structure of the San Andreas fault at Parkfield, California. Geology 25, 359–362.

Wallace, R., 1990. The San Andreas fault system, California. U.S. Geological Survey Professional Paper 1515, 283.

Waters, A.C., Campbell, C.D., 1935. Mylonites from the San Andreas fault zone. American Journal of Science 29, 473–503.

Weldon, R.J., Meisling, K.E., Alexander, J., 1993. A speculative history of the San Andreas fault in the central Transverse Ranges, California. In: Powell, R.E., Weldon, R.J., Matti, J.C. (Eds.), The San Andreas fault system: Displacement, Palinspastic Reconstruction, and Geologic Evolution, 178. Geological Society of America Memoir, Boulder, Colorado, pp. 161–198.

Zhang, X., Sanderson, D.J., 1996. Numerical modelling of the effects of fault slip on fluid flow around extensional faults. Journal of Structural Geology 18, 109–119.

Zhao, D., Negishi, H., 1998. The 1995 Kobe earthquake: Seismic image of the source zone and its implications for the rupture nucleation. Journal of Geophysical Research 103, 9967–9986.